BUTTERWORTH HEINEMANN

Polymer Vol. 36 No. 21, pp. 4083–4089, 1995
Elsevier Science Ltd
Printed in Great Britain

Influence of thermal imidization on the crystallization and melting behaviour of the aromatic polyimide, LaRC CPI-2

Don K. Brandom and Garth L. Wilkes*
Department of Chemical Engineering, Polymer Materials and Interfaces Laboratory, Virginia Polytechnic Institute and State University, Blacksburg, VA 24061, USA
(Received 13 January 1995)

The development of crystallinity during the thermal imidization of a rigid aromatic polyimide synthesized from 1,4-bis(4-aminophenoxy-4′-benzoyl)benzene (1,4-BABB) and oxydiphthalic dianhydride (ODPA) was investigated. Film samples were imidized through a stepwise procedure involving isothermal staging for 1 h each at 100, 200 and 300°C. Differential scanning calorimetry (d.s.c.), wide-angle X-ray diffraction (WAXD), small-angle X-ray scattering (SAXS), transmission electron microscopy (TEM) and thermogravimetric analysis (t.g.a.) were employed to monitor changes in the crystalline state of the films during imidization. The development of crystallinity during thermal imidization was shown to progress through stages that depended upon the time and temperature of the process, wherein the final crystalline index was approximately 46%. This relationship was explained in terms of chain mobility. SAXS analysis suggests that a two-stage, lamellar in-filling process exists for the development of the final crystalline superstructure where the final long spacing is approximately 130 Å. Fourier transform infra-red spectroscopy (*FT*i.r.) analysis does not reveal the presence of anhydride groups at any stage of the imidization process, indicating that significant chain scission did not occur during processing. Transmission electron microscopy (TEM) analysis of the stepwise imidized films reveals that crystalline growth begins at the glass surface of the film and progresses toward the air surface with increasing thermal staging. TEM analysis of a series of fully imidized films reveals that an amorphous layer remains at the air surface of the films, the thickness of which is dependent upon molecular weight.

(Keywords: thermal imidization; aromatic polyimide; crystallization)

INTRODUCTION

Owing to their excellent thermal, thermo-oxidative and chemical resistance properties[1–4], aromatic polyimides have gained considerable prominence among the polymers chosen for high-performance applications in both the aerospace and electronics industries. As a class of polymers, polyimides have been historically regarded as amorphous. While many of these amorphous systems are thermally stable (glass transition temperatures in excess of 300°C) they often display poor solvent resistance. Since the introduction of crystallinity serves as an effective means of improving solvent resistance there has been a considerable thrust of research aimed at developing semicrystalline polyimide systems. Strong contributions to this area from the workers at the NASA-Langley Research Center[5–11] have led to a variety of crystallizable polyimide materials. Some of these materials have been investigated for their general structural characteristics as either adhesives or matrix resins for high-temperature composites. One of the crystallizable polyimides developed recently by researchers at NASA-Langley is LaRC CPI-2 (**L**angley **R**esearch **C**enter **C**rystalline **P**olyimide—second generation), the structure of which is shown below.

The glass transition temperature of this rigid aromatic polyimide is ca. 217°C and its repeat molecular mass $M_0 = 759\,\mathrm{g\,mol^{-1}}$. Low-molecular-weight samples of this polymer display dual endothermic (melting) transitions at ca. 334°C and 364°C during differential scanning calorimetry (d.s.c.) analysis. These transitions have been shown to be the result of a lamellar melt-recrystallization phenomenon which is dependent upon molecular weight[12]. The low melting transition is the result of

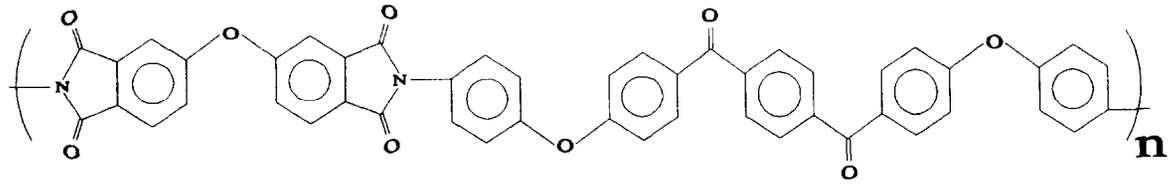

* To whom correspondence should be addressed

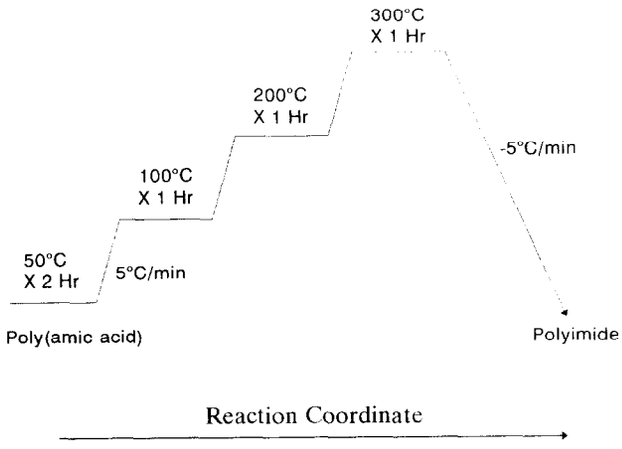

Figure 1 Stepwise thermal imidization profile

Table 1 Sample identification for stepwise thermally imidized films **a** through **i**

Film sample	Temperature (°C)	Time at temperature (h)
a	100	1
b	125	0
c	150	0
d	175	0
e	200	0
f	200	1
g	225	0
h	250	0
i	300	1[a]

[a] Film sample **i** held at 300°C for 1 h plus the −5°C min^{-1} cool down to ca. 50°C

melting relatively 'thin' lamellae which immediately undergo a melt recrystallization to yield thicker lamellae. These 'thick' lamellae then melt at a higher temperature. The synthetic method for the production of these polyimide films involves stepwise thermal imidization of a poly(amic acid) cast from dimethyl acetamide (DMAc) or n-methyl pyrrolidinone (NMP), wherein the film undergoes isothermal staging for 1 h each at 100, 200 and 300°C. This stepwise thermal imidization cycle, originally developed by researchers at NASA[5], has been adopted by many others in the production of a variety of polyimide films[5–10]. Many studies have been conducted to study the mechanisms and side reactions involved during thermal imidization of poly(amic acid)s[13–16]. In the study of the thermal imidization of poly(amic acid) films derived from oxydianiline (ODA) and pyromellitic dianhydride (PMDA), Brekner and Feger[13,14] showed that a complex formed between the poly(amic acid) and the solvent medium, 1-methyl-2-pyrrolidinone (NMP). This interferes with imidization until decomplexation occurs at higher temperatures (ca. 350°C), at which point the newly freed NMP acts as a plasticizer and facilitates imidization. This conclusion is supported through *FT* i.r. studies by Snyder *et al.*[15]. Here a significant presence of side reactions resulted from imidization (of the same polymer–solvent system) at lower temperatures, whereas closed-ring imide formation predominated at higher temperatures (>400°C). Young *et al.*[16] analysed the process of thermal imidization of soluble polyimide films. Here the researchers were able accurately to track molecular weight with degree of imidization in *N*,*N*-dimethylacetamide (DMAc). They found a dramatic reduction in molecular weight during thermal imidization which reached a minimum at temperatures of 150–200°C. As the imidization temperature increased beyond this range, the molecular weight values increased. The final polyimide reaches $\langle M_n \rangle$ values of about 60% of that of the original poly(amic acid) value of 106 000 g mol^{-1}. In a study that investigated many aspects of crystallinity in a semicrystalline polyimide similar in structure to LaRC CPI-2, Pratt *et al.*[17] observed the development of crystallinity in a thermal imidization procedure similar to that currently under study. The development of crystallinity, as calculated from WAXD, appeared to follow a non-linear course with the level of imidization. The objective of this paper is to study the crystalline changes occurring in an aromatic polyimide during a standard stepwise thermal imidization cycle used by the authors within this laboratory, as well as by many others.

EXPERIMENTAL

Synthesis

For the stepwise thermal imidization study 1,4-bis(4-aminophenoxy-4′-benzoyl)benzene (1,4-BABB) (0.01318 mol) was reacted with oxydiphthalic dianhydride (ODPA) (0.01219 mol) and phthalic anhydride (PA) (0.00198 mol) to form a phthalic anhydride endcapped poly(amic acid) with a calculated number-average molecular weight of ca. 9700 g mol^{-1} according to the Carothers relationship[18]. The solids content was 15% (w/w) in dimethyl acetamide (DMAc). The reaction proceeded under a dry nitrogen blanket, at room temperature with stirring, for 27 h. The poly(amic acid) was then removed and centrifuged for approximately 1 h and then cast onto clean, dry Pyrex plates and spread out with a doctor blade set at a 30 mil* gap. The average thickness of the fully cycled films was approximately 7 mil. The films were dried under forced dry air for 18 h at room temperature. Imidization proceeded by placing the films in a Fisher IsoTemp programmable forced air oven for 2 h at 50°C before the oven was heated at 5°C min^{-1} to 300°C with 1 h isothermal holds at 100, 200 and 300°C. The oven was then allowed to cool at −5°C min^{-1} to ca. 50°C. A schematic diagram representing this thermal profile is shown in *Figure 1*. Film samples labelled as **a**–**i** were removed at specific stages during the imidization process, as shown in *Figure 1* and *Table 1*. It is a necessary consequence of the removal of film samples during the imidization process that the oven environment is temporarily disturbed. This disturbance was minimized through rapid sample removal and minimal ambient air exposure to the chamber. At temperatures higher than 250°C the oven could not recover quickly from the heat lost during sample removal. Hence, no samples were taken beyond 250°C until the cycle was complete and the final sample **i** was removed at room temperature. The films were removed from the Pyrex plates by soaking in water at ca. 50°C for approximately 1 h. The films were then allowed to air

* 1 mil = ~25 μm

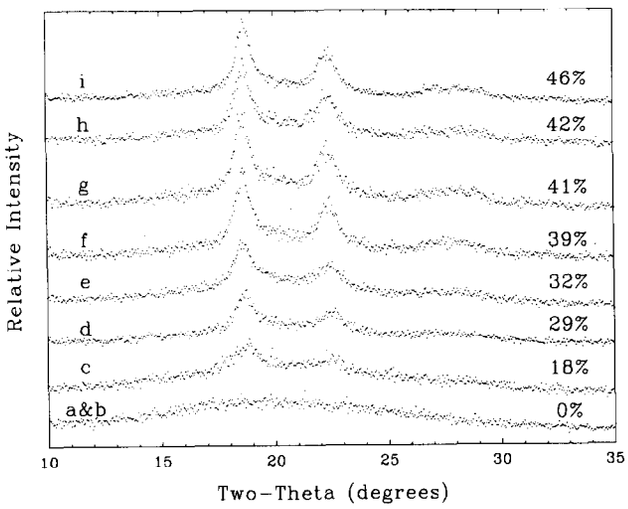

Figure 2 Wide-angle X-ray diffraction (WAXD) scans of thermally staged films **a** through **i**

dry. Other LaRC CPI-2 films discussed in the TEM section of this paper were synthesized in the same fashion as described above with the same imidization temperature and heating rates. Monomer stoichiometric offset was employed to obtain films with calculated molecular weights of 30 000, 15 000 and 7200 g mol^{-1}.

Characterization

Differential scanning calorimetry (d.s.c.) was performed on 5–7 mg film samples using a Seiko DSC model 210 under a nitrogen purge of 20 ml min^{-1} at a heating rate of 20°C min^{-1}. Thermogravimetric analysis (t.g.a.) was performed on a Seiko TGDTA model 200 under a nitrogen purge of 20 ml min^{-1} from room temperature to 600°C at a heating rate of 5°C min^{-1} using ca. 10 mg samples. Wide-angle X-ray analysis was performed on stacked polyimide film samples (three to five layers) using a Nicolet model Stoe/V-2000 X-ray diffractometer using CuKα radiation with a wavelength of 1.54 Å. Two θ values from 3° to 40° were scanned at 0.05° steps with a 10 s dwell. Smeared small-angle X-ray (SAXS) profiles were taken from stacked polyimide film samples (three to five layers) using a slit-collimated compact Kratky camera equipped with an M. Braun position-sensitive detector. The X-ray source was a Philips PW-1729 generator providing Ni-filtered CuKα radiation with a wavelength of 1.54 Å. Bright-field TEM images were obtained from a Philips model 1L 420T STEM. No staining of the films was necessary since the textures were readily visible without a staining agent, as reported earlier for the similar LaRC CPI-1 system[19]. Air and glass surfaces were distinguished by embedding duplicate film specimens in epoxy with the air surfaces facing one another. The film samples were microtomed perpendicular to the film plane in the usual fashion on a Reichert-Jung Ultracut E43 equipped with a diamond knife.

RESULTS AND DISCUSSION

Ideally the degree of imidization would be quantified for all stages of this stepwise process. Fourier transform infra-red spectroscopy (*FT*i.r.) analysis is typically employed to achieve this objective by tracking the development of the characteristic imide band at ca. 1777 cm^{-1}. For quantitative results the *FT*i.r. spectra must be normalized to some peak that is unaffected by the chemical changes occurring during imidization. In a study tracking thermal and microwave imidization in an aromatic polyimide containing ketone and ether connecting groups, Kishanprasad and Gedham[20] normalized the spectral intensity using an aromatic absorption band at 1500 cm^{-1}. In the present study it was found that the reaction solvent, DMAc, presented a peak which greatly overlapped this 1500 cm^{-1} aromatic band. No other available i.r. bands, common to both the imide and amic acid, were left unaffected by the imidization process. Hence, quantification of the degree of imidization was not possible in the LaRC CPI-2 system. It was noted, however, that the presence of an anhydride band, at ca. 1850 cm^{-1}, was not found in any of the film samples. This indicates that there was no significant amount of chain scission occurring during the imidization process, as has been noted by some researchers[16,19].

Wide-angle X-ray diffraction (WAXD) was employed in order to quantify the changes in the amount of crystallinity during imidization. A common procedure for the determination of the degree of crystallinity in polymers is known as the method of Hermans and Weidinger[21,22]. Here, several WAXD scans of a polymer with differing amounts of crystallinity are normalized with regard to their X-ray optical density and the incoming beam intensity. The areas corresponding to the crystalline and amorphous halo regions are then determined by forming a demarcation line between the amorphous and crystalline regions. These areas are used to solve a set of linear equations in which the areas for the 100% crystalline and 100% amorphous material can be determined. The linearity of the relationship between the crystalline and amorphous areas is used to confirm the validity of the technique and accuracy of the results. Further confirmation is presented in terms of the match between the mathematically determined 100% amorphous area and the area from a completely amorphous sample. In the present study the optical densities of the film samples were very low and small fluctuations in beam intensity greatly disrupted the normalization values for the scans. Consequently, the desired linear relationship was not achievable. Lacking this internal validation, great care was taken to use a consistent method for the demarcation between the crystalline and amorphous regions. A single amorphous halo profile that best fitted all diffractograms (when scaled to the proper intensity) was chosen in order to eliminate errors introduced by changing curve shapes. All integrations were taken from 2θ values of 11–35°. The reproducibility of this method to estimate the level of crystallinity was found to be ±2%. It should be noted that the crystalline percentage values presented here do not represent absolute values but, rather, provide an index of the crystallinity. The self-consistent method, however, allows for the determination of trends in crystallinity.

Figure 2 shows the WAXD patterns for the thermally staged films. The first evidence of crystallinity appears in the 150°C imidized film, sample **c**, whereby the analysis just described provided 18% crystallinity. The crystalline content increases significantly along the reaction coordinate to about 39% at stage **f** (200°C for 1 h). Thereafter,

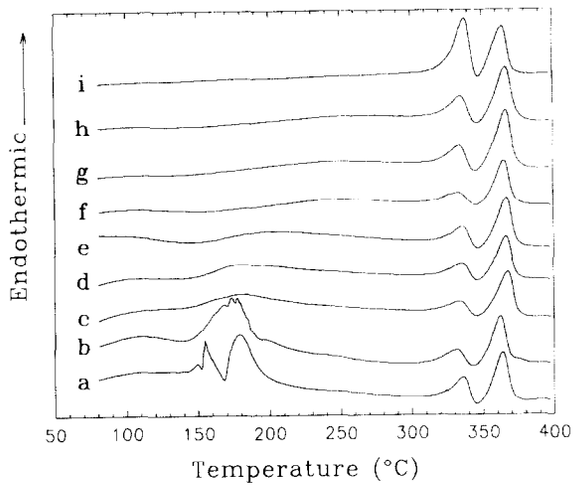

Figure 3 Differential scanning calorimetry (d.s.c.) thermograms for the thermally staged films **a** through **i**

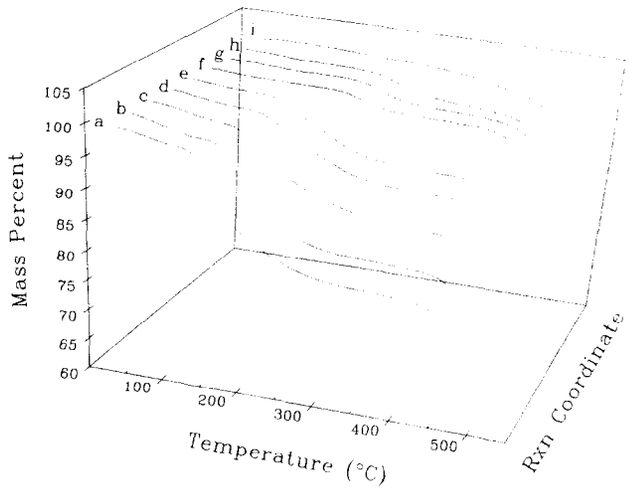

Figure 4 Thermogravimetric analysis thermograms of the thermally staged films **a** through **i**

only gradual changes occur until the final stage is reached and the crystalline fraction increases by a modest jump of 4 to 46% crystallinity for sample **i**. It is notable that a considerable increase in crystallinity occurs during the 1 h staging at 200°C.

D.s.c. of the series of films reveals complex changes occurring in the films in the sub-melting temperature range of the least imidized films (*Figure 3*). In the 150–200°C temperature range the thermograms of films **a** and **b** display large multiple transitions, while at higher temperatures the dual melting transitions characteristic of this polyimide are evident. Since these films were completely amorphous before d.s.c. analysis, it is clear that a crystallization process occurred during heating in the DSC. T.g.a. scans of the series of films, shown in *Figure 4*, reveal a mass loss beginning in the 150°C region for the least imidized films which shifts to progressively higher temperatures with increasing imidization. The significant weight loss of approximately 20% for films **a** and **b** in the 150–200°C region correlates well with the multiple transitions seen for these films in the d.s.c. traces. Thus, these transitions are believed to be caused by a combination of several overlapping endothermic and exothermic events. Most assuredly, solvent loss and crystallization are occurring, which may also be accompanied by imidization. It is noteworthy that there is a dramatic difference in the t.g.a. loss profiles for the two 200°C film samples. Sample **e**, taken at the beginning of the 200°C isotherm, loses considerable mass below 200°C. Sample **f**, held at 200°C for 1 h, begins to lose significant mass in the 225°C region. This parallels a considerable increase in the crystallinity from 32 to 39%. Thus, during this isothermal hold at 200°C, solvent is lost with a concurrent increase in the crystallinity.

In general, it is apparent that the magnitude of the changes in crystallinity at each stage paralleled the weight loss profiles for the film samples. The crystallization process that began between 125 and 150°C steadily increased the crystalline fraction until the film had been held for 1 h at 200°C (sample **f**). Here a plateau was reached, at about 40% crystallinity, where only modest changes in crystallinity occurred by processing to 250°C (sample **h**). The t.g.a. thermograms clearly show a significant weight loss for the samples leading up to sample **f**, corresponding to the region where the greatest increases in crystallinity occurred. Similarly, a plateau in the weight loss curves is noted for samples **f**–**h**, see *Figure 4*. The modest difference in the t.g.a. loss profiles between sample **h** and the fully imidized sample **i**, parallels the modest increase in crystallinity of about 4%. Since the total weight loss due to the water of imidization is only of the order of 5%, it is safe to relate the t.g.a. profiles primarily to solvent loss. The correspondence between weight loss and crystalline development can be attributed to the mobility of the polymer chains. In the stages that show dramatic changes in crystallinity, residual solvent caused a plasticization effect that provided greater chain mobility, thereby allowing crystallization to proceed. Concurrently with this effect, the glass transition temperature of the polymer undoubtedly increased as imidization proceeded. Thus, a combination of a low glass transition temperature and plasticization promoted dramatic crystallization changes in the early stages of the thermal treatment. As solvent was lost and imidization proceeded, chain mobility was restricted and crystalline changes were less dramatic.

SAXS analysis provides an interesting insight into the development of the crystalline superstructure during the imidization process. *Figure 5* shows SAXS profiles of the stepwise imidized films plotted as the smeared intensity as a function of s, where $s = (2/\lambda)\sin(\theta/2)$, λ is the wavelength and θ is the radial scattering angle. The curve representing samples **a** and **b** shows only an exponentially rising curve at low s values, consistent with the fact that there are no scattering centres. Samples **c** through **i** all show a scattering profile where the peaks for samples **e** through **i** are better defined. Qualitatively it can be seen that the 'peak' positions are located at very low s values for films **c** and **d**, corresponding to a relatively high long spacing. The peak position for sample **e** is found at a higher s value (shorter long spacing) with samples **f** through **h** then having their peak positions at a still somewhat higher s value. The peak position then shifts back to a lower s value for sample **i**.

Given that the scattering centres for these curves are lamellar in texture with the lateral length very much greater than the thickness (at least two orders of

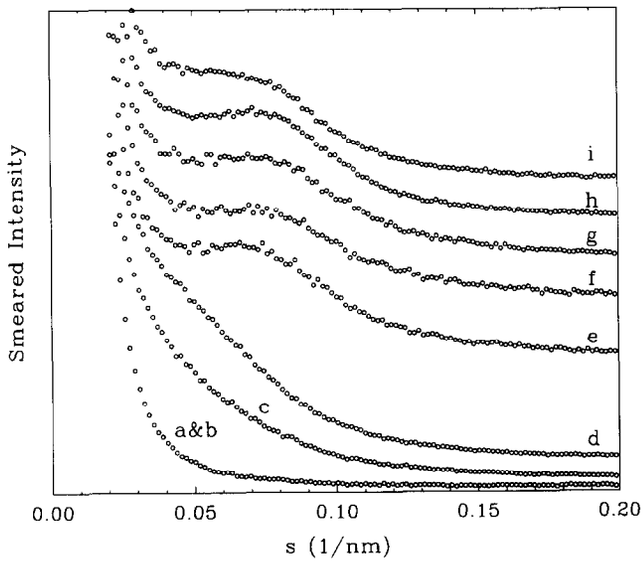

Figure 5 Small-angle X-ray scattering (SAXS) scans for the thermally staged films **a** through **i**

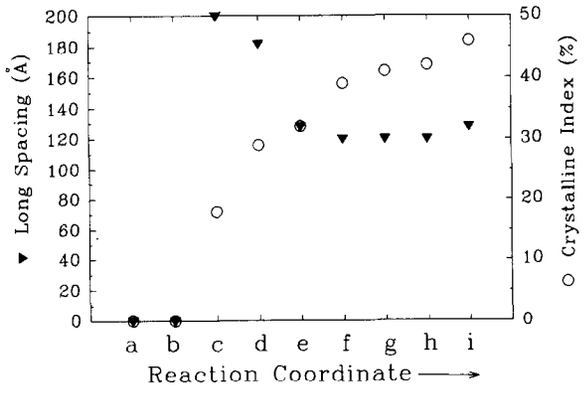

Figure 6 Results of SAXS and WAXD analysis showing the long spacing and crystalline index, respectively

magnitude), it is appropriate to apply the Lorentz correction for platelike structures. This operation corrects the scattered intensity for the random orientation of the lamellar plates (with respect to the X-ray beam) and the amount of actual radiation observed as a result of an intersection of the scattered radiation (in reciprocal space) with the Ewald sphere[23–25]. In this case of lamellar plate scattering from slit-smeared SAXS data, the Lorentz correction is a multiplier of s, that is, $I(\text{corr}) = I(\text{obs})s$. A consequent effect of this correction is an enhanced peak resolution which allows for a more quantitative comparison of the long spacings discussed above. Analysing the peak positions thus created, one finds that the long spacing is quite large for the low-crystallinity samples **c** and **d** (200 Å and 180 Å, respectively). the long spacing drops dramatically for sample **e** to about 130 Å. Samples **f** through **h** all exhibit long spacings of the order of 120 Å. As a result of the final staging of the films the long spacing increases slightly to a value of about 130 Å for sample **i**. *Figure 6* shows these trends in the long spacing along with the changes in bulk crystallinity. A possible explanation for the dramatic drop in long spacing may be found in terms of a lamellar in-filling (insertion) process and/or a contraction of the amorphous phase. In the earliest stages of crystalline development, below 29%, widely spaced lamellae are formed about 200 Å apart in sample **c** and 180 Å in sample **d**. As the degree of crystallinity increases, lamellae are inserted between the previously formed lamellae, dramatically lowering the long spacing to about 130 for sample **e** and 120 Å for samples **f** through **h**. A lamellar insertion mechanism of this kind was first proposed by Keller[26] to explain a drop in SAXS long spacing during isothermal crystallization of isotactic polystyrene. A similar drop in long spacing was found by Hsiao *et al.*[27] during the isothermal crystallization of poly(aryl ether ketone). Here also a lamellar insertion mechanism was used to explain the results. In the present case a contraction of the amorphous phase between adjacent lamellae during imidization and crystallization may also be occurring, which could help account for these results. The increase in long spacing in the final stage may be the result of an isothermal lamellar thickening process, wherein the distance between the scattering centres is increased slightly.

TEM analysis reveals that the crystalline superstructure development is non-uniform. The superstructure appears to develop at the glass surface of the film and progress upward with increasing thermal staging, with some spherulites isolated in the amorphous layer above the crystal growth front. This would imply that the glass acts as a nucleating surface and a self-nucleation process occurs as the crystal growth front progresses toward the air surface. In all the film samples, excepting sample **i**, a sizeable amorphous layer (approximately 4–25% of the film thickness) exists at the air surface. In sample **i** the amorphous layer is very thin, of the order of 1 μm, which is less than 0.5% of the film thickness. *Figure 7A* and *B* shows TEM cross-sections for samples **h** and **i**, respectively. The crystalline and amorphous regions are near the air surface of the films. The arrows indicate the vertical direction from the glass to air surface. The considerably larger amorphous layer in the incompletely staged film **h** is readily apparent (approximately 10–13 μm). The 'filling-in' of the amorphous layer with crystal superstructure in the last thermal stage corresponds well with the final increase in crystallinity for sample **i**. It is notable that there exists a large amorphous layer in the early staged samples where the crystalline index is low. For example, in sample **c** approximately 20–25% of its thickness is amorphous. Thus, the crystalline index for that part of the possessing crystalline superstructure is actually much higher (of the order of 24%).

Previous studies into the crystallization and melting behaviour of LaRC CPI-2 revealed a strong dependence of the level of crystallinity upon the molecular weight of the polymer[12]. Thus, one would expect the progressive development of crystallinity from the glass to the air surface also to depend upon molecular weight, that is, higher molecular weight samples should have larger amorphous zones at their air surface because of an overall lower rate of crystallization. TEM cross-sections of fully imidized films with varying molecular weights, as calculated from the Carothers relationship, showed that the expected trend is present (TEM micrographs not shown). The amorphous layer thickness, along with the percentage of the total film thickness of approximately 10 to 14 mil, for the fully imidized films ranked along

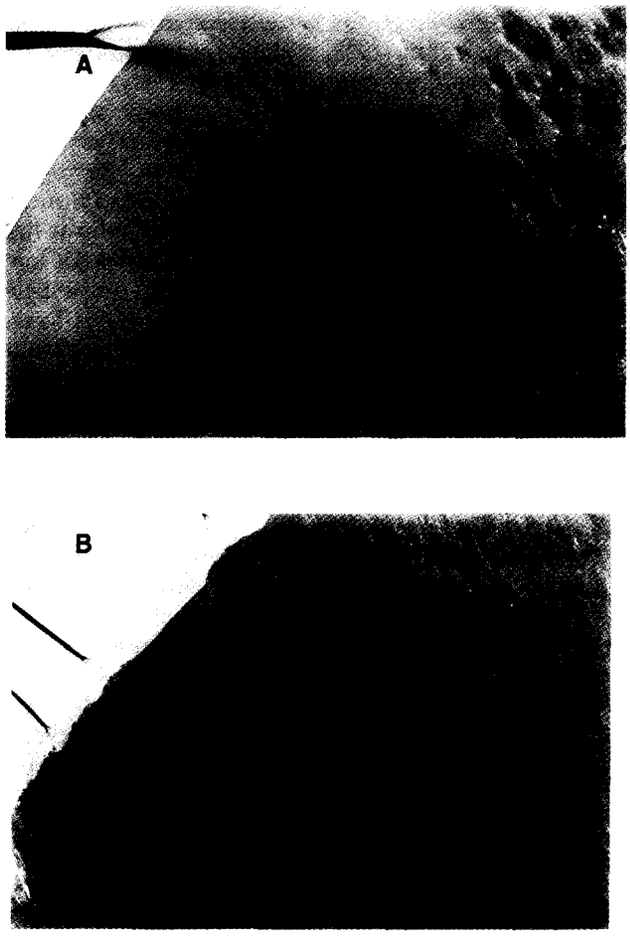

Figure 7 TEM micrographs of cross-sections of samples (A) **h** and (B) **i**. The crystalline and amorphous regions are near the air surface of the films. The arrows indicate the vertical direction from the glass to air surface

with sample **i** was: 15 μm (5%), 4 μm (1.3%), 1 μm (0.3%) and 0.5 μm (0.15%) for films with calculated molecular weights of 30000, 15000, 9700 and 7200, respectively. All of these films were produced in the same fashion, including the percentage solids concentration at the time of casting the poly(amic acid)s. Presumably differing solvents, solids concentrations and temperature profiles would have an effect on the extent of the amorphous layer. It may be noted here that a necessary consequence of a final film product possessing a thin amorphous layer on the surface might well be an inherent susceptibility to chemical attack at that surface.

SUMMARY

The development of crystallinity during thermal imidization of a LaRC CPI-2 film was shown to progress through stages that depended upon the time and temperature of the process. The magnitude of the changes in crystallinity paralleled the weight loss profiles for the film samples. This relationship was explained in terms of chain mobility. Crystalline development began between 125°C and 150°C with a final increase in crystallinity to 46% noted in the last stage of the process. There appear to be only gradual increases in crystallinity during imidization at 200°C for 1 h, 225°C and 250°C. This is consistent with less chain mobility due to less available solvent at these stages, along with the fact that significant conversion has already taken place. At no stage during thermal imidization was the 1850 cm^{-1} anhydride peak found, indicating that no significant chain scission occurred. SAXS analysis suggests that a two-stage process exists for the development of the crystalline superstructure. In the first stage, occurring below 200°C, widely spaced lamellae are formed. Crystallization then proceeds by inserting lamellae between previously formed lamellae and/or incorporation of amorphous material between lamellae into the crystalline phase. Subsequently, a thickening of the lamellae occurs in the final stage. The development of crystalline superstructure begins at the glass surface of the films and progresses upward towards the air surface. The glass surface appears to act as a heterogeneous nucleation site with subsequent self-nucleation of new superstructures. An apparently amorphous layer remains on the air surface of LaRC CPI-2 films produced as described in this paper. The extent of this layer is dependent upon the molecular weight of the polymer.

ACKNOWLEDGMENTS

The authors appreciate the support of this research by the National Aeronautics and Space Administration under contract number NGT-51117. The support of the National Science Foundation Science and Technology Center for High Performance Adhesives and Composites at Virginia Tech under contract number DMR8809714 was greatly appreciated. The authors would also like to thank Paul Hergenrother, Dr Steven Havens and Dr Heather Brink for their guidance regarding polyimide synthesis. TEM work performed by Steve McCartney was sincerely appreciated.

REFERENCES

1 Mittal, K. L. (Ed.). 'Polyimides, Synthesis, Characterization, and Applications', Vol. 1, Plenum Press, New York, 1984
2 Hergenrother, P. M. *Encycl. Polym. Sci. Eng.* 1987, **7**, 639
3 Cella, J. A. *Polym. Degrad. Stabil.* 1992, **36**, 99
4 Hergenrother, P. M. *Angew. Chem. Int. Edn. Engl.* 1990, **29**, 1262
5 Bell, V. L., Stump, B. L. and Gager, H. *J. Polym. Sci.* 1976, **14**, 2275
6 Progar, D. J., Bell, V. L. and St. Clair, T. L. US Pat. 4065345 (1977)
7 Bell, V. L. US Pat. 4094862 (1978)
8 Hergenrother, P. M., Wakelyn, N. T. and Havens, S. J. *J. Polym. Sci., Polym. Chem. Edn.* 1987, **25**, 1093
9 Hergenrother, P. M. and Havens, S. J. *J. Polym. Sci., Polym. Chem. Edn* 1989, **27**, 1161
10 Hergenrother, P. M., Beltz, M. W. and Havens, S. J. *J. Polym. Sci: Part A: Polym. Chem.* 1991, **29**, 1483
11 Havens, S. J. and Hergenrother, P. M. *J. Polym. Sci.: Part A: Polym. Chem.* 1992, **30**, 1209
12 Brandom, D. K. and Wilkes, G. L. *Polymer* 1994, **35**, 5672
13 Brekner, M. and Feger, C. *J. Polym. Sci.: Part A: Polym. Chem.* 1987, **25**, 2479
14 Feger, C. *Polym. Eng. Sci.* 1989, **29**(5), 347
15 Snyder, R. W., Thomson, B., Bartges, B., Czerniawski, X. and Painter, P. C. *Macromolecules* 1989, **22**, 4166
16 Young, P. R., Davis, J. R., Chang, A. C. and Richardson, J. N. *J. Polym. Sci.: Part A: Polym. Chem.* 1990, **28**, 3107
17 Pratt, J. R., St. Clair, T. L., Gerber, M. K. and Gautreaux, C. R. in '*Polyimides: Materials, Chemistry and Characterization*' (Eds C. Feger *et al.*), Elsevier Science, New York, 1989, p. 193

18 Carothers, W. H. *J. Am. Chem. Soc.* 1929, **51,** 2548
19 Muellerleile, J. T., York, G. A. and Wilkes, G. L. *Polym. Commun.* 1991, **32,** 176
20 Kishanprasad, V. S. and Gedham, P. H. *J. Appl. Polym. Sci.* 1991, **50,** 419
21 Hermans, P. H. and Weidinger, A. *Makromol. Chem.* 1961, **44–46,** 24
22 Weidinger, A. and Hermans, P. H. *Makromol. Chem.* 1961, **50,** 98
23 Alexander, L. E. 'X-ray Diffraction Methods in Polymer Science', John Wiley, New York, 1969
24 Balta-Callejá, F. J. and Vonk, C. G. 'X-ray Scattering of Synthetic Polymers', Polymer Science Library, Vol. 8, Elsevier, Amsterdam, 1989
25 Crist, B. and Morosoff, N. *J. Polym. Sci., Polym. Phys. Edn* 1973, **11,** 1023
26 Keller, A. IUPAC Int. Symp., Macromol. Proc. Florence, 1980, pp. 135–179
27 Hsiao, B. S., Gardener, K. H., Wu, D. Q. and Chu, B. *Polymer* 1993, **34,** 3986